

Statistical Inferences on Tree Swallow Migrations, Using Random Forests

Tim Coleman¹, Lucas Mentch¹, Daniel Fink², Frank La Sorte², David Winkler², Giles Hooker³, and Wesley Hochachka²

¹*University of Pittsburgh, Department of Statistics*

²*Cornell Lab of Ornithology*

³*Cornell University, Department of Statistics*

Abstract

Species migratory patterns have typically been studied through individual observations and historical records. In this work, we adopt a data-driven approach to modelling the presence of the North American Tree Swallow (*Tachycineta bicolor*) throughout the eastern United States, using data collected through the eBird project at Cornell University's Lab of Ornithology. Preliminary models suggest a qualitatively different pattern in Tree Swallow occurrence between the years of 2008-2009 and 2010-2013. We implement a global hypothesis test based on the functional predictions of Random Forests (RFs) to evaluate whether this effect is significant or not. In order to better understand the effect of climate change, we also conduct a test evaluating the effect of daily maximum temperature anomaly in predicting tree swallow occurrence. We implement a local test using the asymptotic normality of the predictions of a modified RF, which relies on subsampled trees. This test is conducted at 6 locations in space throughout the northeastern U.S. Finally, we present visual evidence that maximum temperature is affecting the predictions of RF models via a “heat map” of the differences in RF predictions. We also demonstrate that there is a spatial pattern in the effect using Moran's I statistic.

1 Introduction & Motivation

Tree Swallows are migratory aerial insectivores. In a breeding season study [Winkler et al., 2013] established how the maximum daily temperature during the breeding season affected the abundance of the flying insects Tree Swallow feed on. This local-scale study (conducted in Ithaca) established how cold snaps, defined as two or more consecutive days when the maximum temperatures did not exceed 18.5C, resulted in lower abundance of flying insects, and, how in turn, temperature indirectly led to lower fledgling success.

The goal of this study is to determine if local-scale variation daily maximum temperature also affects patterns of occurrence in Tree Swallow populations across broader biogeographic extents. To test this, we decided to study Tree Swallow population during the autumn migration when Tree Swallows are believed to be facultative migrants. Facultative migration is an opportunistic migration strategy where individuals migrate in response to local conditions, like the prevailing food supplies or weather conditions. The region that we decided to study, is the low elevation New

England / Mid-Atlantic Coast stretching north from the Chesapeake Bay to Boston (Bird Conservation Region 30) that forms the northern extent of the Tree Swallow winter range. Anecdotal accounts from birders in this region suggest that Tree Swallows inhabit this region only during relatively warm winters.

Assuming that the same local-scale variation in daily maximum temperature affects food availability for Tree Swallows throughout the study region during the autumn, we expect to see a number of measurable population-level outcomes. We have organized four of these expected outcomes from more general region-wide effects to more specific local-scale effects:

1) We should see year to year variation in Fall occurrence rates across this region. During the study period, there were years where temperatures were generally warmer or colder region-wide. Averaged across the region, we expect this variation in temperature to result in detectable changes in occurrence rates of the species (Changes in intra-annual trajectories)

2) Averaged across the region throughout the autumn, we expect that decreases in temperature should generally result in decreasing occurrence rates (Marginal effect estimate). Based on [Winkler et al., 2013] we expect this relationship to be strongest (i.e. the steepest part of a partial effect estimate) at 18.5C or colder. We expect that the strongest effect may occur at colder temperatures because the Winkler et al. study was done during the summer when temperatures are generally warmer.

3) The ecological effects of temperature can be localized at small spatial scales. Consider microhabitats where the effects of temperature are moderated by local land cover classes (e.g. open fields vs forest) or modified by elevation. For this reason, we expect the effects of temperature to also vary at smaller spatiotemporal scales within the extent of the study. We are not sure how exactly the effect of temperature should vary or be modified by other factors, like day of the year, elevation, or land cover. We think of this a hybrid hypothesis in the sense that we expect temperature to interact with other factors, but we dont know exactly how. One way to test this is by looking for spatiotemporal interactions with temperature, without looking for particular interactions between max temp and other predictors.

4) More specifically, we expect that the effect of temperature to be most pronounced at the very end of the migration. This is when Tree Swallows have left the inland areas and occur only in coastal wetlands. This is the time when the population will be most sensitive to cold snaps, which finally force Tree Swallows to leave these areas and migrate further south.

We are interested in predicting the probability of tree swallow occurrence (referred to from here as just occurrence) as a function of several ecological and spatial indicators. We restricted our attention to only observations within Bird Conservation Region 30 (BCR30), because of the large amount of data available and the strong seasonal change in the region in the Fall. The transitional behavior of migratory birds that is of the most interest, because bird populations are often most vulnerable at these times. Figure 1 plots the spatial extent of BCR30, which covers much of the coastal Mid-Atlantic and New England.

2 Hypotheses of Interest

We begin by summarizing questions of interest that motivated this paper:

- Are there statistical differences between yearly patterns in tree swallow occurrence?
- How does temperature play a role in tree swallow migration?

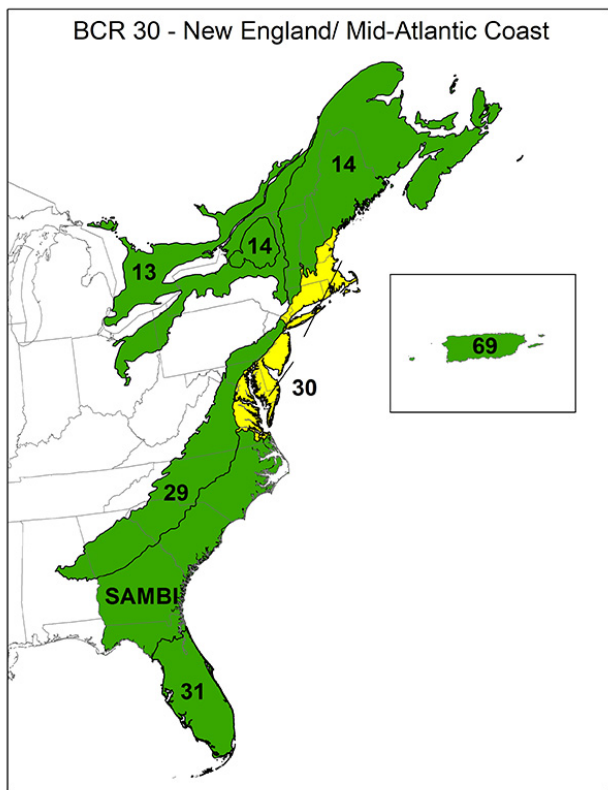


Figure 1: Map of the eastern US highlighting BCR30. Source: <http://acjv.org/wp-content/uploads/2015/01/BCR30.jpg>

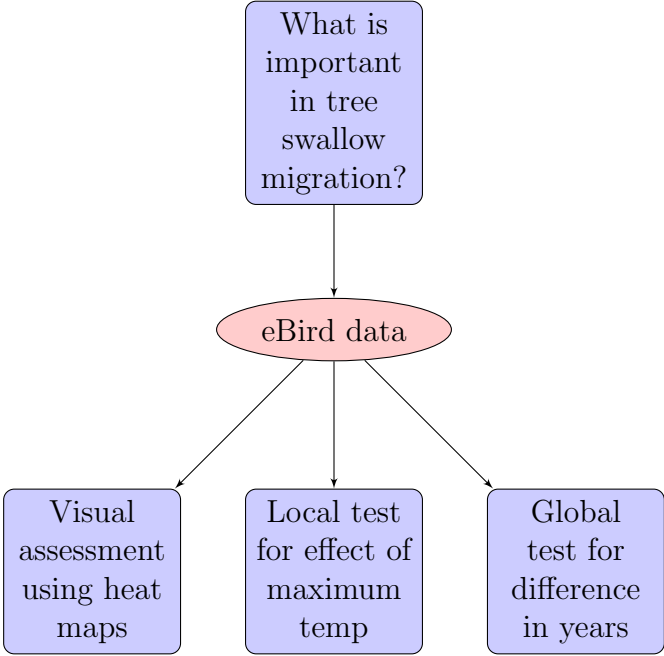


Figure 2: Flow chart summarizing the approach in this paper.

- Do flexible methods, such as Random Forests (RFs), capture the qualitative patterns one would expect in tree swallow migration?

We address the first bullet through treating the RF regression function as a single observation of functional data, and then testing for differences between regression functions trained on different training sets. To address the second bullet, we use a formal approximate test described in [Mentch and Hooker, 2016] to test for the significance of maximum temperature at a variety of test locations through BCR30. Finally, we analyze the difference in predictions of a RF trained with and without maximum temperature. We produce maps in differences of predictions to understand the spatial patterns in the effect of maximum temperature. Figure 2 summarizes this three-pronged approach.

3 Data

We included three general classes of predictors in our species distribution models: 1) spatial predictors to account for spatial patterns, 2) temporal predictors to account for trends, and 3) predictors that describe the observation/detection process. These last predictors are included in order to account for variation in detection rates, a nuisance when making inference about species distributions.

Spatial information is captured by land cover and elevation data. To account for habitat-selectivity each eBird location has been linked to the remotely-sensed MODIS global land cover product (MCD12Q1) [Friedl et al., 2010]. We used 2011 MODIS land cover data, a static snapshot of the landcover. The 2011 MODIS landcover predictors were associated with eBird observations, collected from 2004 to 2012. We use the University of Maryland (UMD) classification scheme [Hansen et al., 2000]. The UMD scheme classifies each 500m pixel as one of the following 14 classes:

Variable	Indicator
Water	0
Evergreen Needleleaf forest	1
Evergreen Broadleaf forest	2
Deciduous Needleleaf forest	3
Deciduous Broadleaf forest	4
Mixed forest	5
Closed shrublands	6
Open shrublands	7
Woody savannas	8
Savannas	9
Grasslands	10
Croplands	12
Urban and built-up	13
Barren or Sparsely Vegetated	16

Table 1: Land Cover indicators in the predictor set

For this analysis we summarized the land cover data as the proportion of each land cover class within a 3.0km x 3.0km (900 hectare) pixel centered at each location using FRAGSTATS [McGarigal et al., 2012]. Summarizing the land cover information at this resolution reduces the

impact of erroneous land cover classifications and accounts for the motility of birds. Moreover, this resolution means that land cover characteristics should be robust to location misspecification by eBird users.

Elevation defines basic abiotic and biotic constraints that influence species distributions. To account for the effects of elevation, each eBird location is associated with the 30m gridded elevation from the ASTER Global Digital Elevation Model Version 2.

Temporal information is included at three resolutions. At the finest temporal resolution, the observation time of the day is used to model variation in availability for detection; e.g., diurnal variation in behavior, such as participation in the dawn chorus [Diefenbach et al., 2007], may make species more or less conspicuous. The day of the year (1-366) on which the search was conducted is used to capture day-to-day changes in occurrence, and, similarly, the year of the observation is included to account for year-to-year differences.

Temperature data was collected from the DayMet project hosted by Oak Ridge National Lab [Thornton et al., 2017]. The data included daily maximum (max temp), minimum, and mean temperature for each day in the training period. Each eBird location in time and space was referenced with a particular day in the DayMet dataset. We also calculated a “normal” max temp for each day, which was the mean maximum temperature for eBird location from 1980-2007. The anomaly relative to this maximum (max temp anomaly), is of particular interest.

There are three user effort variables included in the model to account for variation in detection rates: the hours spent searching for species (`eff.hours`), the length of transects traveled during the search (`eff.dist`), and the number of people in the search party (`no.obs`). In addition, an indicator of observations made under the traveling count protocol was included to allow the model to capture systematic differences in species detection between the the traveling and stationary counts.

Preliminary Models

The challenge that we face in this study, is how to test the effects of maximum daily temperature while accounting for the other processes that we know have strong effects on species distributions. Species distributions are known to respond to a variety of ecological and physical factors across a range of spatial and temporal scales including climate, weather, elevation, land cover, etc. Moreover, almost all of the data used to study species distributions across broad geographic extents are themselves subject to numerous biases and extraneous sources of variation common with large observational data sets.

This makes RFs an attractive methodology to account for numerous sources of variation using covariates that describe the ecological, physical, and observation processes. The ability of RF to adaptively fit complex additive and interaction effects, means that we can generate distribution models with high predictive performance and models that can adapt to global, as well as local effects. Additionally, we can conduct statistical inference to quantify uncertainty and test hypotheses. Together, RFs open up the possibility of discovering subtle effects of temperature as it interacts with other features of environment to affect species distribution at different times and locations. For many of the tests presented, we implement a RF with `mtry` (the number of predictors in each random subset at each node) maximized. This means that all predictors are available at every split. This RF implementation is typically referred to as *bagging*, or bootstrap aggregation of individual regression trees.

A primary goal of this work is to investigate which features are important in predicting occurrence. A natural candidate covariate is temperature, which is strongly correlated with the day of

the year. As mentioned earlier, the eBird data comes with daily maximum, minimum, and mean temperature of the geographical location of a sighting. Motivated by the findings of [Winkler et al., 2013], we restricted our attention to maximum temperature anomaly, because of the insectivorous nature of tree swallows. Typically, insect activity is more strongly determined by daily maximum temperature than by features like mean 24-hour temperature. Insect activity determines the food available for tree swallows, and therefore maximum temperature should be a strong predictor of occurrence.

RF models, first described in [Breiman, 2001], are ensemble learners noted for their ability to attain high predictive accuracy on datasets with large numbers of predictors. We split the BCR30 Tree Swallow data into observations from 2008-2009 and 2010-2013, in order to create training and test sets that are temporally separated. Annual occurrence plots (not included) had suggested these groupings based off qualitative differences in the plot. The 2008-2009 data has 21907 observations, while the 2010-2013 has 151095. We trained a full RF on each of the divided

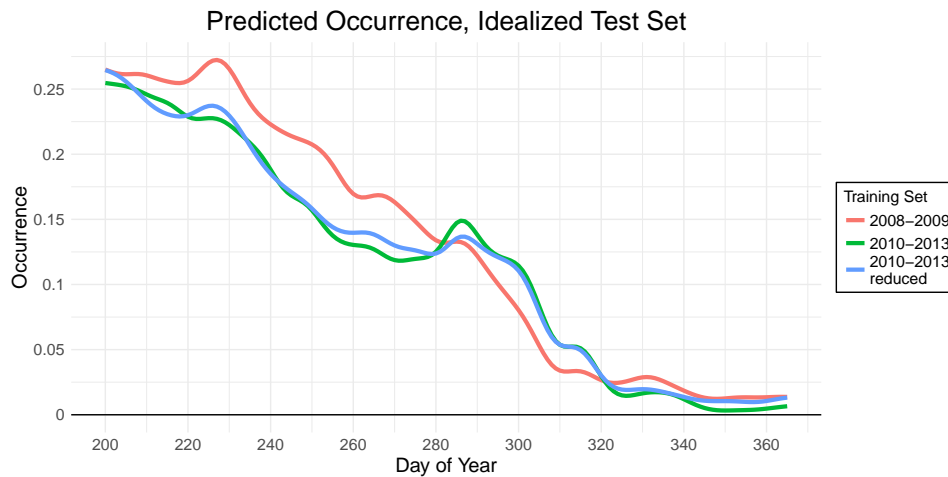


Figure 3: Occurrence fit to data using three different random forests, each trained on a different training set. Also shown are kernel smoothed estimates of the prediction surface, with a Gaussian kernel and bandwidth = 5

training sets. To control for the effect of differing sample sizes, we also fit a RF to a subset of the 2010-2013 data of size equal to that of the 2008-2009 data. For each day in the year, we held out 100 points at random to serve as the idealized test set. These points were removed from all three training sets, to be “true” test points. Finally, predictions were made at all 16600 points, and averaged by day. The results are summarized in Figure 3. We do see a qualitative difference between the two groups, even when taking the reduced 2010-2013 dataset into account. Therefore, differences in random forests trained on different datasets could yield insight into the features that are important in predicting occurrence.

One focus of this work is on using a RF model to draw inferences about the significance of maximum temperature. We calculated a partial effect (of maximum temperature) function for a forest trained on the entire dataset, with day of year removed as a predictor. These plots are generated by fixing a level of maximum temperature and averaging over all predictions made on data in that level. The results of this are shown in Figure 4. Indeed, we see a steady increase in occurrence with maximum temperature. The sharpest increase occurs around 15 degrees Celsius, which [Winkler et al., 2013] showed corresponds to a period of heightened insect activity. We

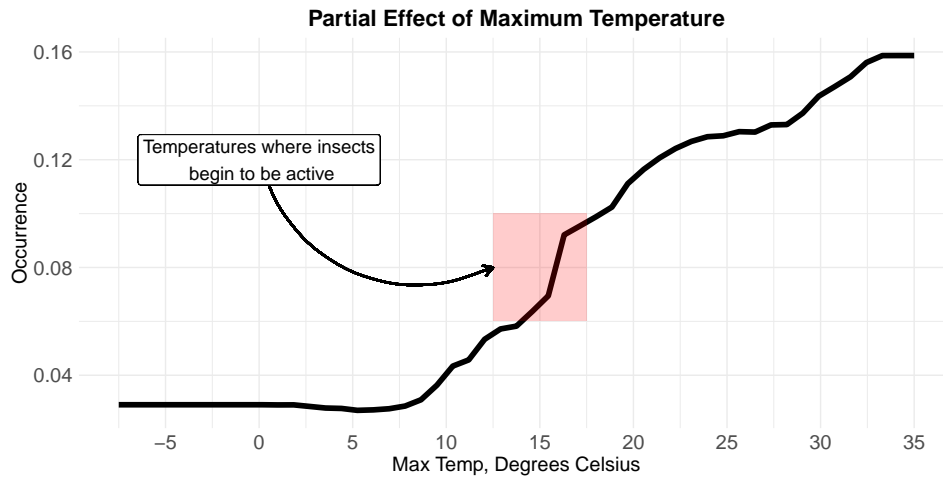


Figure 4: Partial effects plot for maximum temperature for a RF trained on the entire dataset

also see a strong sigmoidal response to maximum temperature, which suggests that maximum temperature has a strong effect.

Maximum temperature is likely significant no matter what collection of years are examined. The question of interest is whether the temperature patterns of 2008-2009 were associated with the qualitative differences observed in Figure 3. As such, we are interested in how anomalous each collection of years is. Figure 5 shows the mean daily max temperature anomaly for each day of Fall. We see that 2008-2009 are generally above 2010-2013 until around DOY 260. There is a peak in 2010-2013 anomaly around DOY 270, which may have the delayed effect of creating the peak at DOY 285 in Figure 3. We see a sharp decline in anomaly around DOY 305 in the 2008-2009 data, corresponding to the steepest decline in occurrence in Figure 3.

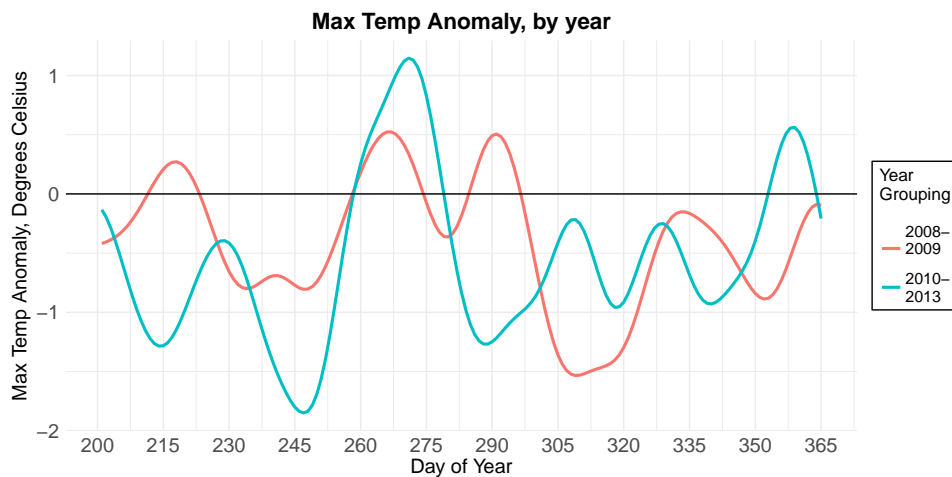


Figure 5: Average max temperature anomaly for each day of Fall, grouped into 2008-2009, 2010-2013. Measured in C.

Finally, we calculated out-of-bag importance for the RF that produced Figure 4. This plot (not included) suggested that maximum temperature was indeed the most important variable, but this conclusion has no inferential value. [Breiman, 2001] introduced out-of-bag importance as a means of

quickly conducting variable selection using random forests, by calculating the performance gains on a test set (such as the out-of-bag data for each tree) of each tree in the forest. However, [Tološi and Lengauer, 2011], [Nicodemus et al., 2010], and [Strobl et al., 2007] demonstrated the problems with relying on these importance calculations; namely that they favor groups of correlated covariates, and that a particular predictors’ ranking in the importance plot is volatile.

4 Methods

Throughout this work we use the regression implementation of RF’s. Because occurrence is a binary random variable, we are predicting the probability of occurrence. Quantifying uncertainty in regression RF’s is an area of active research. Non-parametric resampling methods (such as the jackknife and bootstrap) were used in [Wager et al., 2014] to generate confidence intervals for the predictions of RF’s. Feature significance in the classification context is more challenging, and so we approach predicting occurrence as a regression problem. We apply a resampling based test for significance in the second section, and an asymptotic test in the third section.

4.1 Mapping the Effects of Maximum Temperature

We are interested in examining the spatio-temporal effect of maximum temperature on predicted occurrence. We train two random forests, one with max temp left as is, and another with max temp permuted. Then, we generate an idealized test set, and make predictions at these points. In particular, we use the grid of points used to generate the eBird heat maps as our test points. We restrict our attention to the 3km grid within the $[-78^\circ, -68^\circ] \times [37^\circ, 44^\circ]$ longitude/latitude region. We then make predictions using both forests, and calculate the difference between the predictions. Formally, let y_{ij} be the value of the map at grid cell ij , and let \mathbf{x}_{ij} be the vector of predictors at grid cell ij . Then:

$$y_{ij} = g(\mathbf{x}_{ij}) - g^{(R)}(\mathbf{x}_{ij}) \tag{1}$$

Where g is the unpermuted forest and $g^{(R)}$ is the permuted forest. We supplied 9 test grids, each 20 days apart, throughout the Fall, to examine temporal dynamics too. Ideally, we are looking for spatial patterns in the differences in predictions. Under the assumption that maximum temperature is itself noise, we might expect that the differences in predictions of a permuted and unpermuted forest across space are also independent noise. However, spatial correlations (such as elevation, etc.) in the test set may be reflected in the predictions at the test points. We formally test the hypotheses for spatial correlation between differences in predictions:

$$H_0 : \text{cov}(y_{ij}, y_{i'j'}) = 0 \quad i \neq i', j \neq j' \tag{2}$$

$$H_1 : \text{cov}(y_{ij}, y_{i'j'}) \neq 0 \quad i \neq i', j \neq j' \tag{3}$$

To test this, we first define a distance matrix between points in the grid. Because our grid has 34936 points, a pairwise distance matrix of all points exceeds the memory of a standard computer. To resolve this issue, we take only every 6th point in the grid, and calculate the pairwise distance of the remaining 5822 points. These points are evenly dispersed, and are therefore assumed representative of the entire map. Finally, we use an inverse distance weight:

$$w_{ij,i'j'} = \frac{1}{d_{ij,i'j'}} \tag{4}$$

The distance between a point and itself is 0, but we assign $w_{ij,ij} = 0$, as is standard practice. Then Moran’s I is calculated as:

$$I_{\text{obs}} = \frac{N \sum_{ij, i'j'} w_{ij, i'j'} (y_{ij} - \bar{y})(y_{i'j'} - \bar{y})}{W \sum_{ij} (y_{ij} - \bar{y})^2} \quad (5)$$

Where W is the sum of all entries in the weight matrix, and N is the number of grid cells (in our case, 5822). We then calculate the standardized statistic:

$$Z^* = \frac{I_{\text{obs}} - E(I)}{\sigma(I)} \quad (6)$$

Under H_0 , Z^* can be shown to be asymptotically standard normal [Moran, 1948], so we reject H_0 if the calculated test statistic is more extreme than 1.96.

4.2 Testing for Global Differences in Predicted Occurrence

We consider now consider explicitly testing whether the curves observed in Figure 3 are the same. In particular, denote the partial effect curves observed in Figure 3 as $\chi_i(d)$, where $i \in \{\{2008, 2009\}, \{2010, \dots, 2013\}\}$, where d is taken to be the day of the year. Here, the index i indicates the training data used to train the random forests that produced the predictions at our idealized test set. For computational convenience, we constructed a "similarity" training set out of the 2010-2013 data. This training set was built by taking each observation in the 2008-2009 set, finding the observations in the 2010-2013 which were in roughly the same area and same time as the chosen 2008-2009 observation, and then picking an observation at random from these local observations. We wanted roughly the same spatial/temporal distribution of training observations, to examine the independent influence of the other covariates. Specifically, "roughly" the same area means within 2 days of the point, and within 0.2 decimal degrees in both latitude and longitude.

The idealized test set consisted of 166×500 points, with 500 points taken for each day in the Fall. Each day, 1000 locations in a $3\text{km} \times 3\text{km}$ grid are selected at random, and referenced with their land cover and elevation characteristics, as well as a maximum temperature for that day. The maximum temperature information inputted was 1980-2007 normal maximum temperature, provided by DayMet. This means that the temperatures in the test set are different than those used in the training set (which only spans 2008-2013). The variables associated with the eBird user (i.e. `eff.dist`) were set to 1 uniformly. We excluded day of year and maximum temperature anomaly from these RFs, to see if the effect is based on raw maximum temperatures. Globally, we test the hypotheses:

$$H_0 : \chi_1(d) = \chi_2(d) \quad \forall d \in \{1, \dots, D\} \quad (7)$$

$$H_1 : \chi_1(d) \neq \chi_2(d) \quad \text{for some } d \in \{1, \dots, D\} \quad (8)$$

Here, $D = 166$ is the number of days at which we evaluate χ . In Figure 3, we notice that in early fall (DoY 200-265), the 2008-2009 forest is over-predicting the 2010-2013 curve. Later in the fall (DoY 266-310), 2010-2013 over-predicts 2008-2009, and finally as winter (DoY 311-365) sets in,

we see no difference. This leads to three natural sets of hypotheses:

$$H_0 : \chi_1(d) \leq \chi_2(d) \quad \forall d \in \{1, \dots, 65\} \quad (9)$$

$$H_1 : \chi_1(d) > \chi_2(d) \quad \text{for some } d \in \{1, \dots, 65\} \quad (10)$$

$$H_0 : \chi_1(d) \geq \chi_2(d) \quad \forall d \in \{66, \dots, 110\} \quad (11)$$

$$H_1 : \chi_1(d) < \chi_2(d) \quad \text{for some } d \in \{66, \dots, 110\} \quad (12)$$

$$H_0 : \chi_1(d) = \chi_2(d) \quad \forall d \in \{111, \dots, 165\} \quad (13)$$

$$H_1 : \chi_1(d) \neq \chi_2(d) \quad \text{for some } d \in \{111, \dots, 165\} \quad (14)$$

Note that the hypotheses tested in (9)-(14) each require a different test statistic. We opt for a non-parametric permutation test, allowing for straightforward calculation of p-values. In each permutation, we looked at the combined 2008-2009 and 2010-2013 similarity data, and then permuted the **year** covariate, and then once more split among the years. A RF was then trained on each training set, and its predictions calculated on our idealized test set. In addition to generating the permutation distribution of the $\chi_i(d)$ functional data, we generate the permutation distribution of two measures of functional distance:

$$K\hat{S}_\chi = \sup_d |\chi_1(d) - \chi_2(d)| \quad (15)$$

$$C\hat{v}M_\chi = \frac{1}{D} \sum_{d=1}^D (\chi_1(d) - \chi_2(d))^2 \quad (16)$$

For the temporal tests (9)-(14), we calculate the following three test statistics, which are the raw distances between the curves:

$$\Delta_1 = \frac{1}{65} \sum_{d=1}^{65} (\chi_1(d) - \chi_2(d)) \quad (17)$$

$$\Delta_2 = \frac{1}{55} \sum_{d=66}^{110} (\chi_1(d) - \chi_2(d)) \quad (18)$$

$$\Delta_3 = \frac{1}{55} \sum_{d=111}^{165} (\chi_1(d) - \chi_2(d)) \quad (19)$$

(15) refers to a Kolmogorov-Smirnov type statistic, and (16) refers to a Cramer-von Mises statistic. The use of these statistics for two sample functional testing procedures is studied in [Hall and Van Keilegom, 2007]. Let B be the number of permutations generated, and for a test statistic T , let T_i denote T statistic calculated on i^{th} permutation. Finally, let $I(\cdot)$ be an indicator function. Then, we calculate our p-values for (7) according to:

$$\hat{p}_{KS} = \frac{1}{B} \sum_{i=1}^B I(KS_i > K\hat{S}_\chi) \quad (20)$$

$$\hat{p}_{CvM} = \frac{1}{B} \sum_{i=1}^B I(CvM_i > C\hat{v}M_\chi) \quad (21)$$

For the hypotheses in (9)-(14), our p-values are respectively calculated by:

$$\hat{p}_{\Delta_1} = \frac{1}{B} \sum_{i=1}^B I(\Delta_{1,i} < \Delta_1) \quad (22)$$

$$\hat{p}_{\Delta_2} = \frac{1}{B} \sum_{i=1}^B I(\Delta_{2,i} > \Delta_2) \quad (23)$$

$$\hat{p}_{\Delta_3} = \frac{1}{B} \sum_{i=1}^B I(|\Delta_{3,i}| < |\Delta_3|) \quad (24)$$

We for each p-value, we reject the associated hypotheses if the p-value is less than 0.05. The direction of the inequality in (22) - (24) is determined by the hypotheses of interest. For example, in the first part of the Fall, we expect the 2008-2009 curve to be above the 2010-2013 curve, so we expect the observed distance to be larger than the majority of the permuted distances. Note that our initial belief (from the preliminary models) is that we should reject the hypotheses (9) and (11), but fail to reject (13).

We used a parallel implementation of the `randomForest` function from the `randomForest` and `foreach` packages with 40 trees, with a final node size of 15, and `mtry` = 23. This value of `mtry` meant we were using bagging, rather than a truly randomized RF. We opted for bagging so that we could grow fewer trees and still obtain stable predictions. These bagged trees did not include day of year or maximum temperature anomaly, but rather kept the raw maximum temperature as a feature.

4.3 Local Testing using Supervised Random Forests

We now summarize one of the main results of [Mentch and Hooker, 2016]. In particular, they proposed a modification to Breiman’s RF algorithm. A key difference is the use of *subsampling* trees, where each resampling is done without replacement. Moreover, because sampling is done without replacement, each tree sees a subsample smaller than the entire dataset. This modified RF can be shown to produce predictions that are asymptotically normal, if the subsample sizes are kept small compared to the overall sample size. Thus, the difference in two modified forests is also asymptotically normal. This result leads to a hypothesis test for feature significance of the form:

$$H_0 : g^{(R)}(\mathbf{x}) = g(\mathbf{x}) \quad \forall \mathbf{x} \in X_{\text{test}} \quad (25)$$

$$H_a : \exists \mathbf{x} \in X_{\text{test}} \text{ such that } g^{(R)}(\mathbf{x}) \neq g(\mathbf{x}) \quad (26)$$

Here, g refers to the fitted regression function of the full RF, while $g^{(R)}$ is the RF fitted with selected covariates excluded in some way. Then, $\forall \mathbf{x}_i \in X_{\text{test}}$ we calculate the following:

$$\hat{D}_i := \hat{D}(\mathbf{x}_i) = \hat{g}(\mathbf{x}_i) - \hat{g}^{(R)}(\mathbf{x}_i) \quad (27)$$

The collection of these \hat{D}_i , under H_0 , have mean $\mathbf{0}$ and covariance matrix Σ . We implement [Mentch and Hooker, 2016]’s algorithm for fitting these two forests, which also estimates Σ . Then, normal sampling theory gives that, asymptotically:

$$\hat{\mathbf{D}}^T \Sigma^{-1} \hat{\mathbf{D}} \sim \chi_{n-1}^2 \quad n = \text{card}(X_{\text{test}}) \quad (28)$$

Thus, we reject H_0 if the quantity in (28) is larger than the 95th percentile of the corresponding chi-squared distribution.

In our implementation, we are interested in testing the significance of the maximum temperature anomaly. Day of year is kept in the model, in order to separate the effect of temperature and time of year. This means that the “seasonal” component to occurrence is explicitly captured in the covariates. To fit this into the framework described in (25) - (28), for specified test points, we fit one forest with maximum temperature anomaly included, and another with maximum temperature anomaly randomly permuted. Because the test in (25) and (26) only tests for the difference, outright exclusion will almost always lead to a rejection of H_0 , even if the feature itself is noise [Mentch and Hooker, 2016]. Permuting the predictor instead transforms the predictor into noise, allowing us to test a noise variable against one that may have signal.

Under the H_0 , the predictor is an independent covariate, so a permutation should not change that. With this in mind, for a given test set, we calculate a forest with maximum temperature left as is, and a forest with maximum temperature permuted. We then applied the testing algorithm described in [Mentch and Hooker, 2016] to each of our 6 testing groups. To remain consistent with the global test, and to limit the number of trees needed, we again used subsampled bagging. These tests were implemented using the `rpart` package to perform the regression trees.

Test Point Selection

The hypotheses described in 25 and 26 are only valid at fixed test points, so careful selection of the test points is important. In this study, we are interested in drawing conclusions across a variety of locations and times. Thus, we stratified our test points by location, and conducted 6 different tests. The training and test set were selected from points inside wildlife refuge areas. Wildlife refuges areas are of particular interest because they include areas that are resistant to local environmental changes, due to environmental protections in place. Stratifying testing areas helps isolate the effect of large-scale climate change on tree swallow occurrence. We selected 6 groups of 30 test points each, which were removed from the training set. These 6 groups and points are summarized in Figure 6. These points were chosen so that we maintained consistent spatial coverage and so we could compare and contrast the effect of maximum temperature anomaly across the East Coast. The regions directly represented are:

1. Boston Metropolitan Area
2. Central Connecticut
3. Westchester County, New York
4. Western New Jersey
5. Upper Chesapeake Bay
6. Lower Chesapeake Bay

Spatial centers for each of these regions were manually selected, and the test points are a random sample of points within a 0.3 decimal degree radius. While the actual size of these “bubbles” is distorted throughout space, they each had a contained enough points to ensure we had a complete test set. The final training set for these tests consisted of 25276 observations, and the test set consisted of the 180 spatially-stratified observations.

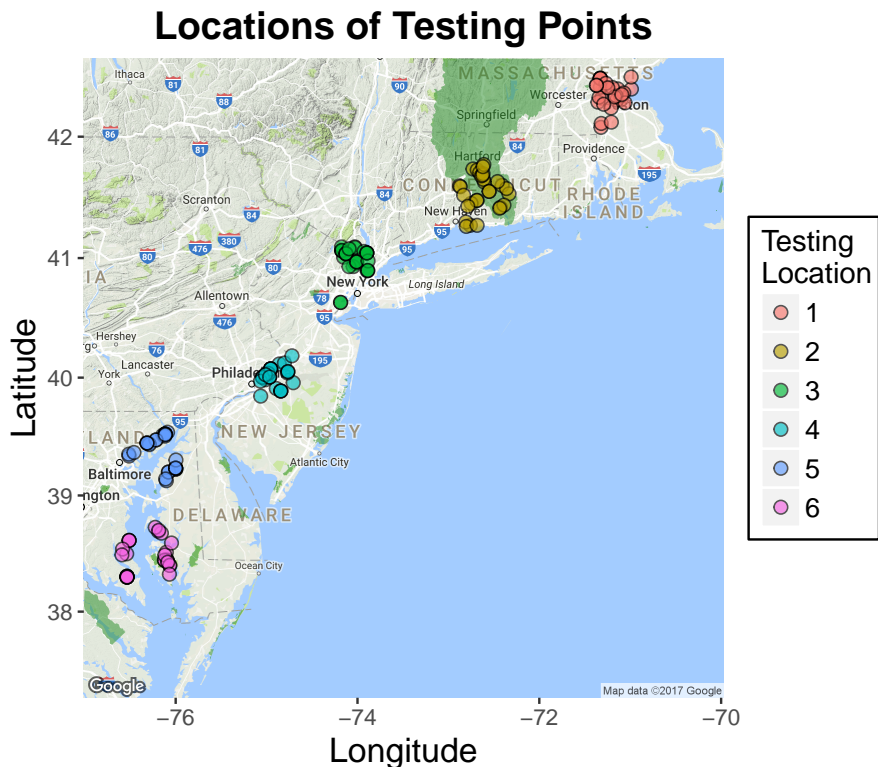


Figure 6: Testing points selected for study. Colors indicate the testing location represented; dots indicate the locations of the test points. Light green overlay indicates Fish and Wildlife Service wildlife refuges. Data provided by GoogleMaps, US Fish and Wild Life. Map created using ggmap [Kahle and Wickham, 2013]

5 Results

5.1 Global Test Results

In Table 2, we report the permutation p-values of the tests of (7), (9), (11), and (13). We see

KS	CvM	Δ_1	Δ_2	Δ_3
0.062	0.070	0.055	0.020	0.711
FTR	FTR	FTR	R	FTR

Table 2: Hypothesis test results for the global test for the various test statistics. The second row is p-values; the third row is the conclusion (FTR = Fail to Reject, R = Reject)

that we fail to reject every hypothesis except for (11). This is not to say that the null hypotheses tested here are necessarily true; the other p-values, except for \hat{p}_{Δ_3} , are all only slightly above 0.05. Moreover, the plots in Figure 7 suggest that the difference is observed most strongly early in the year, where 2008-2009 has higher occurrence than 2010-2013. Then, in the middle of Fall,

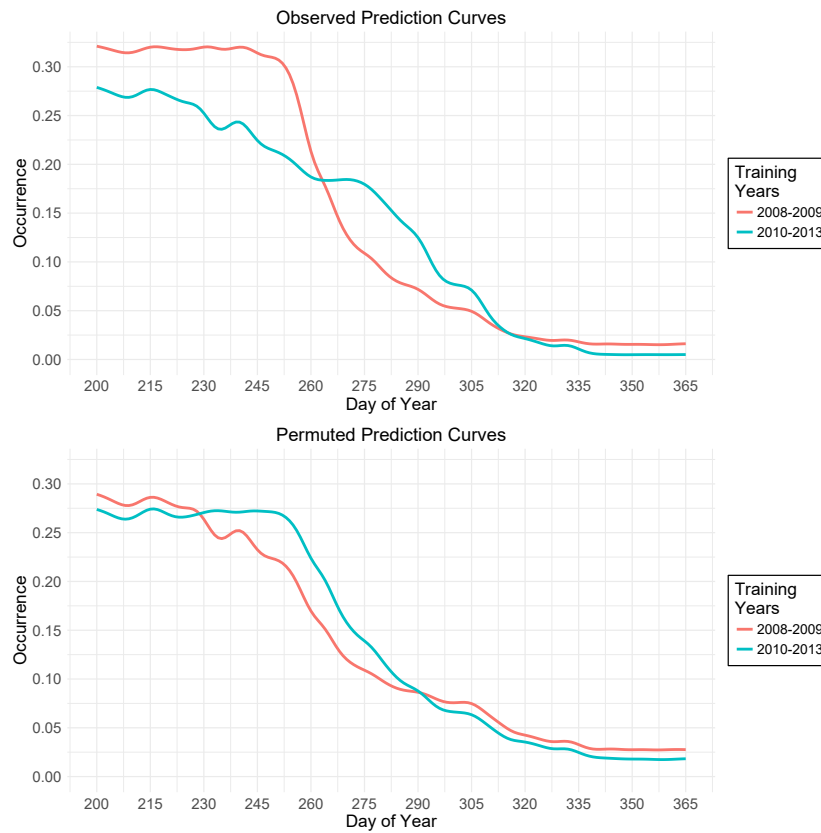


Figure 7: **Top:** Smoothed predicted occurrence curves for the 08-09 training set and the 10-13 training set. **Bottom:** An example of the predicted curves generated after permuting the years. Smoothing done using a Gaussian kernel with a bandwidth of 7.5

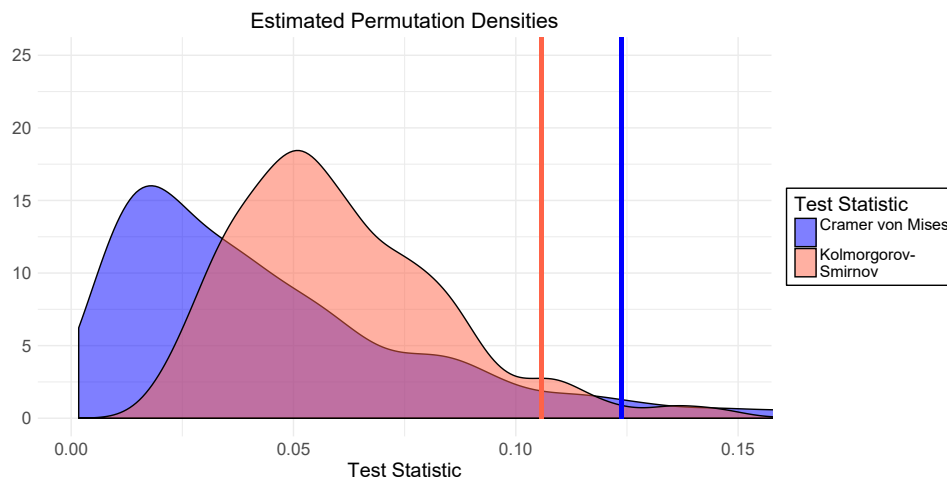


Figure 8: Permutation densities of the Kolmogorov-Smirnov and Cramer von Mises statistics, for the unsmoothed prediction curves. The CvM statistic has been scaled by 50 to accommodate simultaneous plotting. Observed values are shown as vertical lines.

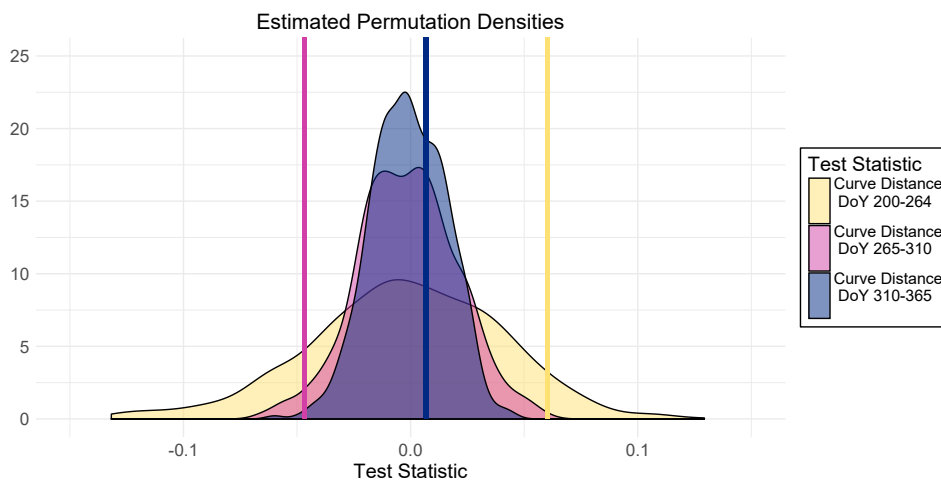


Figure 9: Permutation densities of the test statistics Δ_1 (yellow), Δ_2 (magenta), and Δ_3 (purple). Observed values are shown as vertical lines in colors corresponding to the density colors.

2010-2013 has higher occurrence, and finally there is no visible difference as temperatures drop in the winter. This pattern reflects our understanding from the initial hypotheses. Finally, a fail to reject for Δ_3 affirms our belief that there is no real difference later in the Fall.

5.2 Local Test Results

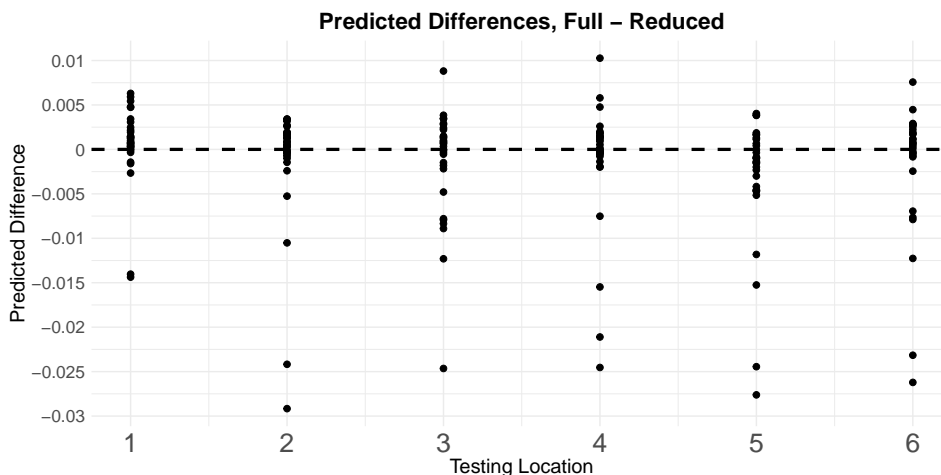


Figure 10: Differences in bagged/RF predicted occurrence for all 180 test points (Full - reduced)

Table 3 summarizes the test statistics and p-values for our observations. We have strong evidence at all locations that maximum temperature is important. Figure 10 shows the predicted differences between the full and reduced models. Though all locations are significant, most of the points have 0 difference, but at least one point has a non-zero difference. This emphasizes that (26) does not state that max temp anomaly has an effect uniformly at each point, rather that at least one point there is a difference.

Testing Location	Test Statistic	P-Value
1	84.51	4.346E-07
2	98.57	3.119E-09
3	102.93	6.373E-10
4	160.10	0.000E+00
5	180.11	0.000E+00
6	89.59	7.585E-08

Table 3: Test statistics for the hypotheses (25) - (26) at the points show in Figure 6

5.3 Maximum Temperature Effect Map

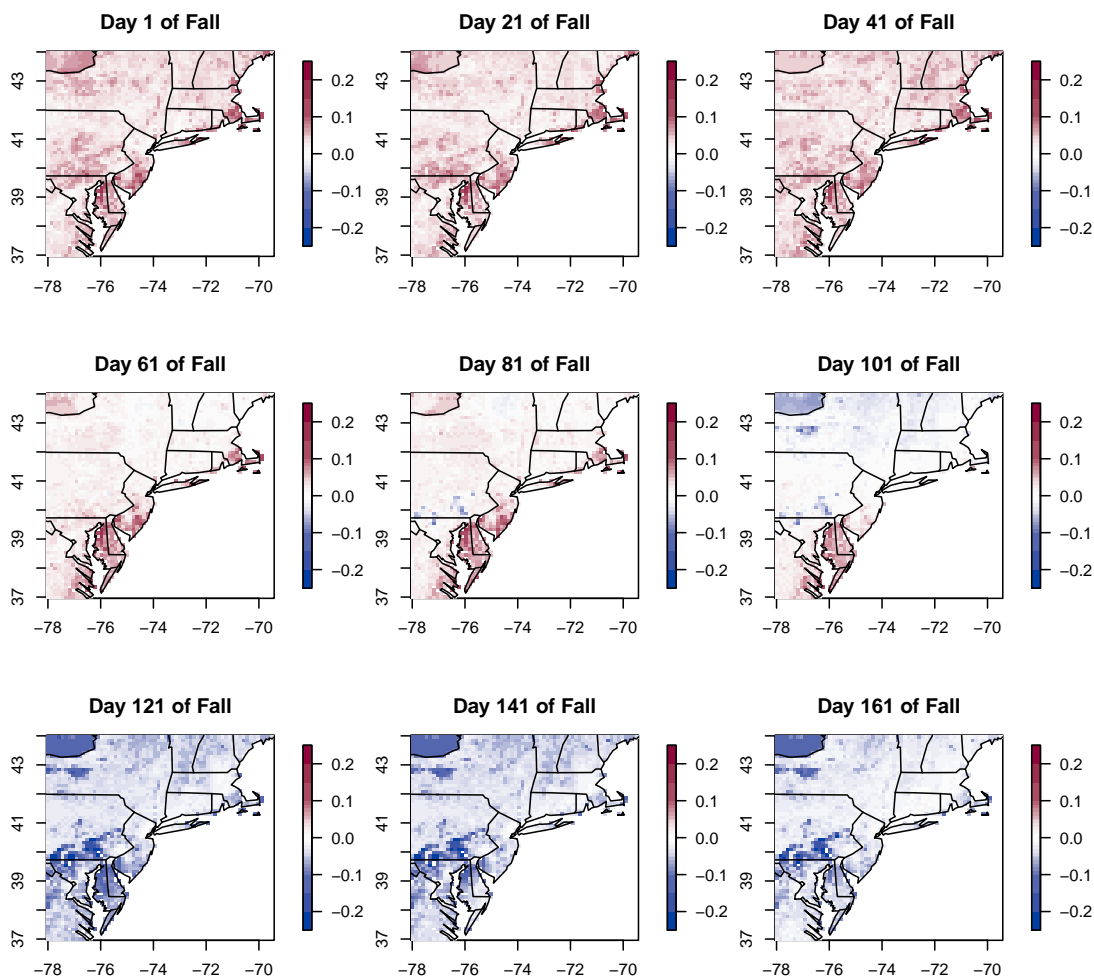


Figure 11: Differences $(g(\mathbf{x}) - g^{(R)}(\mathbf{x}))$ between predicted occurrence for a forest with max temp permuted and max temp unpermuted, calculated at 9 difference instances in the Fall. Red indicates the unpermuted RF predicting higher than the permuted forest, blue indicates the permuted forest predictions being higher. Units are Occurrence.

Figure 11 presents the “heatmap” of the effect of maximum temperature. Red indicates the

permuted RF being higher than the permuted RF, blue indicates the permuted forest being higher. Table 4 presents the results of the Moran’s I test conducted on the spatial data mapped in Figure 11. The Z values are calculated as:

$$Z = \frac{\hat{I} - E(I)}{\sigma(I)} \quad (29)$$

In words, this is the first column minus the second column, all divided by the third. Note that under H_0 (the assumption of no autocorrelation), $E_0(I) = \frac{-1}{N-1}$, [Moran, 1950]. We see that all I values are positive, suggesting that the predictions are strongly correlated throughout space. In Figure 11, we see that there is certainly a “clumping” effect, suggesting that maximum temperature’s effect has a local component.

Day	Observed I	Expected I	Std Error	P value	Z
Day 1	0.0422	-0.0002	0.0004	0.0000	113.4010
Day 21	0.0407	-0.0002	0.0004	0.0000	109.4391
Day 41	0.0302	-0.0002	0.0004	0.0000	81.2810
Day 61	0.1045	-0.0002	0.0004	0.0000	280.3697
Day 81	0.0757	-0.0002	0.0004	0.0000	203.1577
Day 101	0.1673	-0.0002	0.0004	0.0000	448.4178
Day 121	0.0724	-0.0002	0.0004	0.0000	194.3888
Day 141	0.0638	-0.0002	0.0004	0.0000	171.3538
Day 161	0.0804	-0.0002	0.0004	0.0000	216.1006

Table 4: Moran’s I test for spatial auto correlation for each of the days for which a map was generated.

6 Discussion

We see that the RF models are able to pick up on the qualitative differences between the patterns in the observed years. Permuting the years has a clear visual effect on the idealized predictions, an effect that is somewhat supported by the permutation test. We suspect that the permutation test’s inherently lower power may have led to higher p-values in both situations. More simulations (raising B) could improve power. The top panel in Figure 7 shows how 2008-2009 predict a higher occurrence earlier in the year, followed by a sharp decline around day 60. The 2010-2013 predictions are more stable. The lower panel of Figure 7 shows how the permuted curves move in more or less lockstep, with a slight bias persisting between the curves. Being beholden to a 5% Type I error rate is the primary reason for failing to reject the global hypotheses. We do have sufficient evidence to conclude that there is a difference in the predictions made during days 265-310 of the year. 2008-2009 occurrence declines steeply in this region, while 2010-2013 occurrence declines more slowly, which may explain why we rejected (11). In (9), the levels are substantially different, but the rates of change do not vary strongly until towards the end of the period.

A clear drawback of this testing procedure is having to fit $2B$ forests, which is computationally prohibitive. Because B needs to be large to ensure the test enjoys adequate power, looking for alternative means of testing these hypotheses is of primary interest. Certain “depth” based approaches to functional hypothesis testing may lead to more powerful tests that rely on fewer observations of functional data needed [Geneens, 2017], [Geneens and Nieto-Reyes, 2017].

The local tests for significance of max temperature anomaly suggest that maximum temperature is important in each of the regions tested. The highest test statistics were observed in regions 4,5 which correspond to lower New Jersey and the upper Chesapeake, and the lowest in the lower Chesapeake. From Figure 10, we see in region 1 (Boston Metro Area) how a single stray test point can lead to a significant test statistic. This speaks to the fact that H_0 for the local tests is a very strong condition, and a single point producing an effect is enough to negate H_0 . In Figure 10, we see that most predictions are clustered around 0, with only a few points deviating by more than .01 (i.e. more than 1% chance of observing a tree swallow). Even under peak tree swallow sighting conditions, occurrence only peaks around 25% (Figure 3), so a .01 difference is more significant than at first glance. In general, there's a negative effect on predicted occurrence from permuting maximum temperature anomaly, which may reflect that most points come from earlier in the Fall. Some points included in our idealized test set may have come later in the year (when winter has set in), where anomalous temperatures may be meaningless because tree swallows have already left.

We see a regional difference in occurrence between the permuted and unpermuted forest in Figure 11, which again suggests that maximum temperature is indeed important. Moreover, the results of the Moran's I test gives evidence to the hypothesis that there is a spatial pattern of the effect of maximum temperature. In particular, the original forest, g , tends to predict higher than $g^{(R)}$ earlier in the Fall. Equal predictions are attained around day 60-100, and finally, by winter g underpredicts $g^{(R)}$ substantially. This likely corresponds to the fact that the only covariate changing as Fall progresses is max temp. Because permuted maximum temperature is a realization of noise, the predictions of $g^{(R)}$ are essentially time-invariant. The results of the Moran's I test should be interpreted with caution, however. The predictions, $g, g^{(R)}$, are functions of the test set maximum temperature which is strongly correlated throughout space. This means that the predictions may exhibit correlation regardless of an association of occurrence with maximum temperature, and thus their differences may also exhibit correlations. The hypotheses tested using Moran's I, combined with the results of the local test, both support the same conclusion about the effect of maximum temperature.

7 Conclusions

Originally, we posed three questions of interest. We now restate those questions and include the answers suggested by our methods and results:

- **Q:** Are there statistical differences between yearly patterns in tree swallow occurrence?
A: The years of 2008-2009 have a clear visual distinction from the years of 2010-2013 (Figures 3,7). The global test procedure developed earlier provides moderate evidence for differences between the curves. Visually, there is a qualitative difference in max temperature anomaly patterns between 2008-2009 and 2010-2013, which may explain the observed differences.
- **Q:** How does temperature play a role in tree swallow migration?
A: Maximum temperature anomaly is significant at all 6 locations. We see an effect, even accounting for day of year. We see that a majority of points at a given location have small effect sizes, but a few have large deviations. The effect of temperature therefore may be uneven, even at local scales.
- **Q:** Do flexible methods (such as random forests) capture the qualitative patterns one would expect in tree swallow migration?

A: We see that random forests, Figure 11, rely on maximum temperature to account for time of year. In particular, if maximum temperature is permuted (and day of year is excluded), the predictions remain relatively constant.

The procedures used here are not specific to either tree swallows or a particular feature in the eBird dataset. The framework summarized in Figure 2 can be used to test the significance of features for a variety of migratory species. The computational burden, however, of conducting these procedures remains a primary stumbling block. We now suggest various avenues by which these testing procedures could be improved and streamlined.

The hypotheses tested in (25 - 26) are only technically valid at the test points in the set X_{test} . Moreover, the technical conclusion is that there exists some point at which the predictor makes a difference; not that a difference has been observed at all points. These “pointwise” tests are not wholly satisfying, and developing “uniform” tests for an entire regression surface are of interest. Unfortunately, the computational complexity of estimating the covariance matrix Σ limits the number of testing points that can be used. Because under H_0 , the differences in the forest predictions are asymptotically normal, a Kriging approach could interpolate the difference in forests between test points, providing covariance estimates. [Kleijnen and Van Beers, 2005] showed that a Kriging approach could be used when variances are not constant across interpolation points, if there is a parametric structure assumed to the variances. [Opsomer et al., 1999] developed a procedure for iteratively estimating the variances between points with heteroskedastic variances, regardless of the underlying structure. The variance calculations used in [Mentch and Hooker, 2016] lead to unequal variance estimates, necessitating this sort of approach.

The tests developed for (25-26) are only about the differences in predictions, *not* about the accuracy of the predictions. Thus, we are not concluding that maximum temperature anomaly is necessary a strong predictor of occurrence. While ecological intuition would suggest that max temp anomaly should have be a strong predictor, the tests presented here do not provide direct evidence for that hypothesis. No non-resampling test using the mean squared error on a test set has yet been presented, and remains an area of active research. Resampling procedures can always be used, but suffer from the same issues of the functional test used here (many resamples needed, etc.)

The functional testing procedure proposed in section 4.2 uses only distance between functions to calculate the p-values. More sophisticated procedures could use results from functional analysis and topology. [Nieto-Reyes et al., 2016] developed a notion of functional depth, which measures how “deep” within a functional class \mathcal{F} a particular function f is. [Geneens, 2017], [Geneens and Nieto-Reyes, 2017] developed tests for homogeneity of two samples of functional data, using functional depth. Tests using FD are able distinguish between two samples of 20 functions, which could drastically lower the degree of resampling needed. This approach means we could test more features/interactions between features, across an entire regression surface. This would allow for much fewer iterations needed for a global test of differences between prediction functions. Moreover, this procedure could be applied to the samples of partial effects functions, like the one shown in Figure 4, allowing for another test of feature significance. A sample of partial effect plots of permuted features would be compared against a sample of unpermuted partial effects plots. This functional approach to RF modeling, introduced here, may be the basis for stronger testing procedures.

References

- [Breiman, 2001] Breiman, L. (2001). Random forests. *Machine learning*, 45(1):5–32.
- [Diefenbach et al., 2007] Diefenbach, D. R., Marshall, M. R., Mattice, J. A., and Brauning, D. W. (2007). Incorporating availability for detection in estimates of bird abundance. *The Auk*, 124(1):96–106.
- [Friedl et al., 2010] Friedl, M. A., Sulla-Menashe, D., Tan, B., Schneider, A., Ramankutty, N., Sibley, A., and Huang, X. (2010). Modis collection 5 global land cover: Algorithm refinements and characterization of new datasets. *Remote sensing of Environment*, 114(1):168–182.
- [Geneens, 2017] Geneens, G. (2017). Distance depth-based nonparametric tests for homogeneity of functional data.
- [Geneens and Nieto-Reyes, 2017] Geneens, G. and Nieto-Reyes, A. (2017). On the functional distance-based depth.
- [Hall and Van Keilegom, 2007] Hall, P. and Van Keilegom, I. (2007). Two-sample tests in functional data analysis starting from discrete data. *Statistica Sinica*, pages 1511–1531.
- [Hansen et al., 2000] Hansen, M., DeFries, R., Townshend, J. R., and Sohlberg, R. (2000). Global land cover classification at 1 km spatial resolution using a classification tree approach. *International journal of remote sensing*, 21(6-7):1331–1364.
- [Kahle and Wickham, 2013] Kahle, D. and Wickham, H. (2013). ggmap: Spatial visualization with ggplot2. *The R Journal*, 5(1):144–161.
- [Kleijnen and Van Beers, 2005] Kleijnen, J. P. and Van Beers, W. C. (2005). Robustness of kriging when interpolating in random simulation with heterogeneous variances: Some experiments. *European Journal of Operational Research*, 165(3):826–834.
- [McGarigal et al., 2012] McGarigal, K., Cushman, S., and Ene, E. (2012). Fragstats v4: spatial pattern analysis program for categorical and continuous maps. university of massachusetts, amherst, massachusetts, usa. *goo. gl/aAEbMk*.
- [Mentch and Hooker, 2016] Mentch, L. and Hooker, G. (2016). Quantifying uncertainty in random forests via confidence intervals and hypothesis tests. *The Journal of Machine Learning Research*, 17(1):841–881.
- [Moran, 1948] Moran, P. A. (1948). The interpretation of statistical maps. *Journal of the Royal Statistical Society. Series B (Methodological)*, 10(2):243–251.
- [Moran, 1950] Moran, P. A. (1950). Notes on continuous stochastic phenomena. *Biometrika*, 37(1/2):17–23.
- [Nicodemus et al., 2010] Nicodemus, K. K., Callicott, J. H., Higier, R. G., Luna, A., Nixon, D. C., Lipska, B. K., Vakkalanka, R., Giegling, I., Rujescu, D., Clair, D. S., et al. (2010). Evidence of statistical epistasis between *disc1*, *cit* and *ndell1* impacting risk for schizophrenia: biological validation with functional neuroimaging. *Human genetics*, 127(4):441–452.

- [Nieto-Reyes et al., 2016] Nieto-Reyes, A., Battey, H., et al. (2016). A topologically valid definition of depth for functional data. *Statistical Science*, 31(1):61–79.
- [Opsomer et al., 1999] Opsomer, J. D., Ruppert, D., Wand, M. P., Holst, U., and Hössjer, O. (1999). Kriging with nonparametric variance function estimation. *Biometrics*, 55(3):704–710.
- [Strobl et al., 2007] Strobl, C., Boulesteix, A.-L., Zeileis, A., and Hothorn, T. (2007). Bias in random forest variable importance measures: Illustrations, sources and a solution. *BMC bioinformatics*, 8(1):25.
- [Thornton et al., 2017] Thornton, M., Thornton, P., Wei, Y., Vose, R., and Boyer, A. (2017). Daymet: Station-level inputs and model predicted values for north america, version 3.
- [Toloşi and Lengauer, 2011] Toloşi, L. and Lengauer, T. (2011). Classification with correlated features: unreliability of feature ranking and solutions. *Bioinformatics*, 27(14):1986–1994.
- [Wager et al., 2014] Wager, S., Hastie, T., and Efron, B. (2014). Confidence intervals for random forests: the jackknife and the infinitesimal jackknife. *Journal of Machine Learning Research*, 15(1):1625–1651.
- [Winkler et al., 2013] Winkler, D. W., Luo, M. K., and Rakhimberdiev, E. (2013). Temperature effects on food supply and chick mortality in tree swallows (*tachycineta bicolor*). *Oecologia*, 173(1):129–138.